Supporting Information

Kwon et al. 10.1073/pnas.1216830110

SI Materials and Methods

Mouse Strains and Breeding. All mice and their progeny were allowed ad libitum access to food and water during the course of the experimental period. All protocols used in this study were approved by the Medical College of Wisconsin Institutional Animal Care and Use Committee (IACUC). Heterozygous *Gpsm1*$^{+/-}$ mice were generated as described by Blumer et al. (1). Heterozygous *Pkd1*$^{+/V}$ mice were previously described by Yu et al. (2). Double heterozygous *Gpsm1*$^{+/-}$; *Pkd1*$^{+/V}$ progeny mice were produced by mating the heterozygous *Gpsm1*$^{+/-}$ and heterozygous *Pkd1*$^{+/V}$ mice. Dihybrid crosses of double heterozygous *Gpsm1*$^{+/-}$; *Pkd1*$^{+/V}$ mice were used to generate progeny mice with various *Gpsm1* and *Pkd1* genotypes. PCR genotyping was performed for *Gpsm1* and *Pkd1* using protocols published by Blumer et al. (1) and Yu et al. (2).

Biological Measurements and Tissue Morphometry. Before sacrificing the mice at appropriate time points, the animals were weighed, and blood was collected to measure creatinine, blood urea nitrogen (BUN), sodium, and potassium. Creatinine was measured by mass spectrometry (UAB Biochemical Core). Plasma sodium and potassium was determined by flame photometry (Instrumentation Laboratory 943), and BUN was measured by the Alfa Wasserman chemistry analyzer. Upon sacrifice, both kidneys were harvested to calculate total kidney-to-body weight (KW/BW) ratios. Both the right and the left kidney were cut into two pieces; one half of each kidney was used for immunoblot analysis and the other half was fixed in 10% neutral buffered formalin and paraffin embedded for morphometric analysis. The collection of cyst fluid for measurement of sodium and potassium concentrations and osmolality (model 3300 micro-osmometer; Advanced Instrumentation, Inc.) required the use of both kidneys. Renal morphometry was performed on 4-μM sections stained with hematoxylin & eosin (H&E) using a Hamamatsu NanoZoomer HT (Hamamatsu Photonics KK) digital scanner. The total kidney tissue-to-cystic space surface area of multiple kidney sections at 40× magnification was averaged for each genotype and time point. Image post processing and data analysis was performed using Visiomorph and Microimager software (Visiopharm). The Visiomorph software used automated pixel counting to determine differences between tissue and empty space in the renal cortex and medulla. Subsequently, the area of the remaining kidney tissue was divided by the total area of tissue and empty space.

Renal Immunohistochemistry. Serial sections (4-μm thick) were stained with tubule segment-specific markers, Trichrome, or primary antibodies. In brief, antigen retrieval by tryptic digestion or heating (90 °C) in antigen retrieval solution (IHC World) was performed depending on the primary antibody. The slides were blocked and incubated with a primary antibody, and the appropriate secondary antibody was conjugated with either HRP or alkaline phosphatase as used to visualize the binding. Between each of the steps, the slides were rinsed multiple times in Tris-buffered saline. Segment-specific markers including *Lotus tetragonobulus* agglutinin (LTA; proximal tubule), calbindin-28K (distal tubule), and *Dolichos biflorus* agglutinin (DBA; collecting ducts) were used as previously described by Sweeney et al. (3, 4). Trichrome staining was performed to assess the extent of fibrosis in the kidney tissue. The following antibodies were used to stain the kidney sections: (*i*) proliferating cell nuclear antigen (PCNA; 1:1,000 dilution; Cell Signaling) as a marker for proliferation; (*ii*) α-smooth muscle actin (α-SMA; 1:400 dilution; Sigma) as a marker for cell differentiation and fibrosis; and (*iii*) F4/80 (1:200 dilution; Abcam) as a marker for macrophage infiltration. All kidney sections were subsequently counterstained with H&E and digitized using a Hamamatsu NanoZoomer HT digital scanner in the Pediatric BioBank and Analytical Tissue Core at Children's Research Institute.

To determine the localization of G-protein signaling modulator 1 (GPSM1)/activator of G-protein signaling 3 (AGS3) in the kidney sections, an optimized immunofluorescence protocol was used. In brief, GPSM1 primary antibody generated in our laboratory (5) was used at a 1:100 dilution. DBA was used to identify the collecting ducts in the same sections. Negative controls included the following: (*i*) no primary antibody; (*ii*) no secondary antibody; and (*iii*) primary GPSM1 antibody preabsorbed with the peptide used to generate the antibody. The appropriate secondary antibody was incubated at a dilution of 1:1,000 [Alexa Fluor-488 (GPSM1) and Alexa-Fluor-555 (DBA); Invitrogen] for 60 min at room temperature in the dark. The slides were coverslipped with Vecta Shield Mounting Medium containing DAPI. Images from identical areas on serial sections were captured at 40× using an Olympus BX60 microscope equipped with a SPOT Flex camera (Diagnostic Instruments Inc.).

Electrophysiological Measurements of Polycystin-1/Polycystin-2 Ion Channels. Baseline channel activity of reconstituted polycystin-1 (PC1)/polycystin-2 (PC2) channels in CHO cells was measured using previously published methods (6, 7). The expression of PC1, PC2, and rat GPSM1 was achieved by transfecting CHO cells with a combination of plasmids expressing human *PKD1* (2 μg), mouse *Pkd2* (1 μg), and rat *Gpsm1* (1 μg) using the Polyfect reagent (Qiagen). A GFP-expressing plasmid was cotransfected with the PC1/2 expression plasmids to mark the cells for patch clamping. In some experiments, the bovine GRK2ct expression plasmid was transfected to block Gβγ function. To prevent Gαi activity, pertussis toxin (PTX; 200 ng/mL) was added to the culture media 18–24 h before the electrophysiological measurements were made. The current recordings were acquired with a MultiClamp 700B patch clamp amplifier (Molecular Devices) interfaced via a Digidata 1440 (Molecular Devices) to a PC running the pClamp 10.2 software (Molecular Devices). All currents were filtered at 1 kHz. Test pulses (500 ms each) stepping by 20-mV increments from a holding potential of 0 to 100 to −100 mV were used to generate current–voltage (I-V) relations and to measure current at −100 mV. Whole-cell capacitance (average values ∼6–10 pF) and series resistances (average values ∼2–5 MOhm) were compensated. All of the groups were studied using cells independently transfected on two to three different occasions for all groups except for *hPKD1*/*mPkd2*, *hPKD1*/*mPkd2* + *rGpsm1*, and *hPKD1*/*mPkd2* + *bGRK2ct*2 (six to seven independent transfections).

Statistical Analysis. Data were expressed as mean ± SEM. One-way ANOVA was performed between groups for the immunoblotting experiments, patch clamping, and biological plasma measurements. If a probability value of $P < 0.05$ was obtained, Student-Newman–Keuls postdoc analysis was performed. To analyze KW/BW and cystic disease indices, Kruskal-Wallis one-way ANOVA by ranks was performed. If a probability value of $P < 0.05$ was obtained, Dunn's multiple comparison test was performed.

1. Blumer JB, et al. (2008) Activator of G protein signaling 3 null mice: I. Unexpected alterations in metabolic and cardiovascular function. *Endocrinology* 149(8):3842–3849.

2. Yu S, et al. (2007) Essential role of cleavage of Polycystin-1 at G protein-coupled receptor proteolytic site for kidney tubular structure. *Proc Natl Acad Sci USA* 104(47): 18688–18693.

3. Sweeney WE, Jr., et al. (2003) Combination treatment of PKD utilizing dual inhibition of EGF-receptor activity and ligand bioavailability. *Kidney Int* 64(4): 1310–1319.
4. Sweeney WE, Jr., et al. (2001) Phenotypic analysis of conditionally immortalized cells isolated from the BPK model of ARPKD. *Am J Physiol Cell Physiol* 281(5): C1695–C1705.
5. Regner KR, et al. (2011) Loss of activator of G-protein signaling 3 impairs renal tubular regeneration following acute kidney injury in rodents. *FASEB J* 25(6):1844–1855.
6. Babich V, et al. (2004) The N-terminal extracellular domain is required for polycystin-1-dependent channel activity. *J Biol Chem* 279(24):25582–25589.
7. Hanaoka K, et al. (2000) Co-assembly of polycystin-1 and -2 produces unique cation-permeable currents. *Nature* 408(6815):990–994.

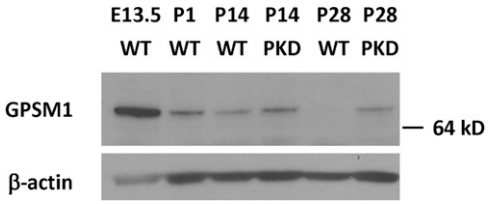

Fig. S1. Temporal expression of GPSM1 protein expression in normal and autosomal dominant polycystic kidney disease mouse kidneys. Representative immunoblot demonstrating GPSM1 protein expression in wild-type (WT) *Gpsm1*$^{+/+}$;*Pkd1*$^{+/+}$ and cystic *Gpsm1*$^{+/+}$;*Pkd1*$^{nl/nl}$ (PKD: polycystic kidney disease) mouse kidneys harvested at different time points. The *Pkd1*$^{+/nl}$ mice were obtained from D. J. Peters (Leiden University Medical Center) (1) and backcrossed to C57BL/6 mice at least five generations by the lab of E. D. Avner (Medical College of Wisconsin) before harvesting kidneys for this experiment. E13.5: embryonic day 13.5; P1, P14, P28: postnatal days 1, 14, and 28, respectively. β-Actin was used as a loading control.

1. Lantinga-van Leeuwen IS, et al. (2004) Lowering of Pkd1 expression is sufficient to cause polycystic kidney disease. *Hum Mol Genet* 13:3069–3077.

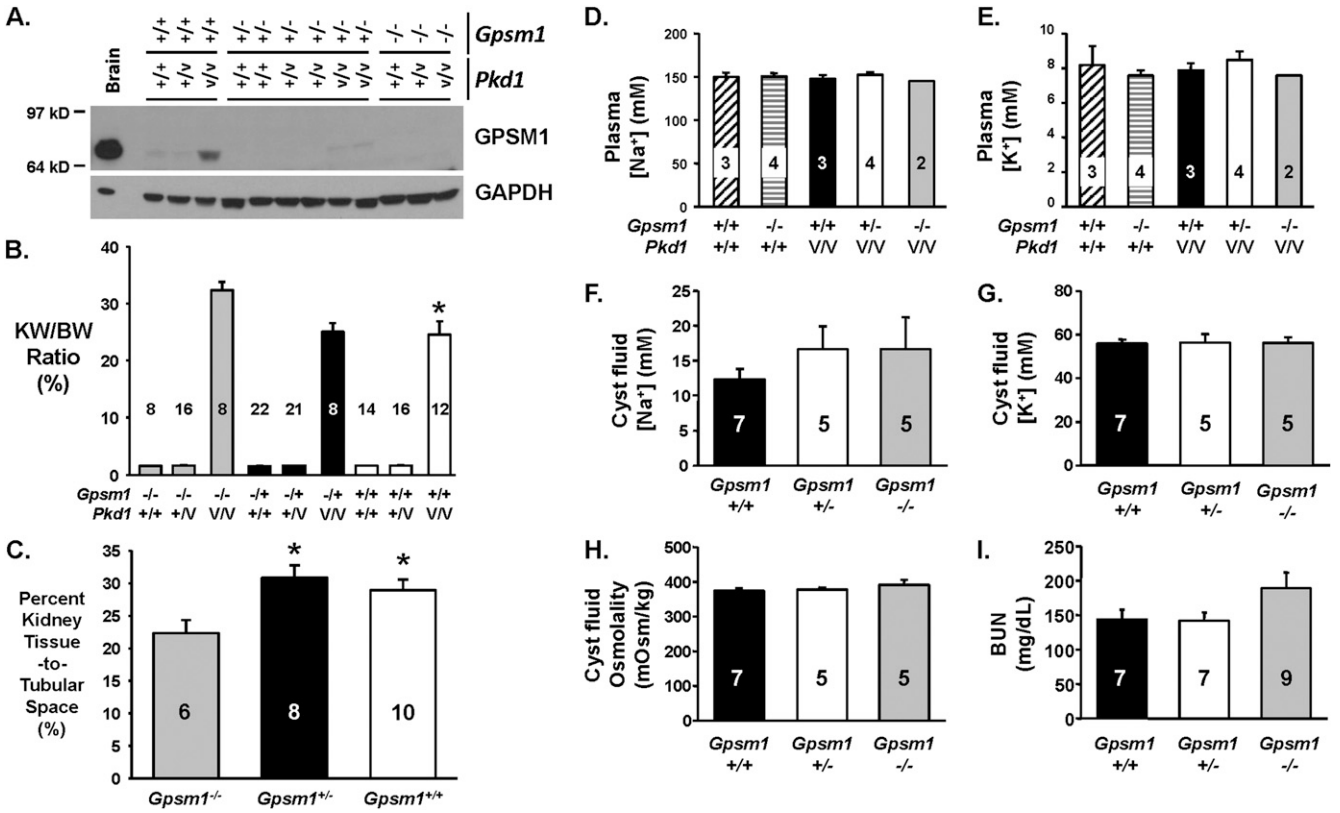

Fig. S2. Renal GPSM1 protein expression and biological measurements in various *Gpsm1;Pkd1* genotyped mouse kidneys obtained at postnatal day 19. $Pkd1^{V/V}$ mice with various *Gpsm1* genotypes were killed at day 19 to measure body weight (BW) and total kidney weights (KW) and for isolation of protein lysates from the kidneys. (*A*) Representative immunoblot analysis of renal GPSM1 protein from various *Gpsm1;Pkd1* mice at postnatal day 19. GAPDH was used as a loading control. Brain (1 μg) was used as a positive control. Cystic $Pkd1^{V/V}$ mice with two functional copies of *Gpsm1* ($Gpsm1^{+/+}$) exhibit higher expression levels than kidneys with only one ($Gpsm1^{+/-}$) or no ($Gpsm1^{-/-}$) functional copy of the *Gpsm1* gene. (*B*) Kidney-to-body weight (KW/BW) ratios were calculated from mice with various *Gpsm1 x Pkd1* genotypes, and the data was graphed as a percentage. The KW/BW ratios of the $Gpsm1^{-/-}$;$Pkd1^{V/V}$ mouse kidneys (32.3 ± 1.4%; n = 8) were higher ($P < 0.05$) than the ratios obtained from the $Pkd1^{V/V}$ mice with a single ($Gpsm1^{+/-}$) or both copies ($Gpsm1^{+/+}$) [i.e., 25.0 ± 1.5% (n = 8) and 24.6 ± 2.3% (n = 12)]. Numbers of mice with each genotype are shown in the graph. *$P < 0.05$: significant difference between $Gpsm1^{+/+}$;$Pkd1^{V/V}$ versus $Gpsm1^{-/-}$;$Pkd1^{V/V}$. (*C*) Kidneys were fixed in 10% neutral buffered formalin, paraffin-embedded, and sectioned for H&E staining. Each of the kidney sections was morphometrically analyzed to determine the surface area of the remaining kidney tissue relative to the tubular (cyst) space, and graphed as a percentage. The percentage of kidney tissue remaining in $Gpsm1^{+/+}$;$Pkd1^{V/V}$ mice [28.9 ± 1.6% (n = 10)] and $Gpsm1^{+/-}$;$Pkd1^{V/V}$ mice [30.8 ± 1.9% (n = 8)] was significantly higher ($P < 0.05$) than in $Gpsm1^{-/-}$;$Pkd1^{V/V}$ mouse kidneys [22.3 ± 2.0% (n = 6)]. In noncystic $Gpsm1^{-/-}$;$Pkd1^{+/+}$ kidney sections, the percentage of kidney tissue surface area-to-tubular space was 91.0 ± 1.4% (n = 5) (data not shown). *$P < 0.05$ significant difference between $Gpsm1^{+/+}$;$Pkd1^{V/V}$ and $Gpsm1^{+/-}$;$Pkd1^{V/V}$ versus $Gpsm1^{-/-}$;$Pkd1^{V/V}$. Plasma electrolyte levels (*D* and *E*) and BUN (*I*) were measured from blood collected from $Pkd1^{+/+}$ and $Pkd1^{V/V}$ mice with various *Gpsm1* genotypes at postnatal day 19. Some of these mice were euthanized to collect cyst fluid from the kidneys to determine electrolyte (*F* and *G*) and osmolality levels (*H*). There was no significant difference in the BUN measurements between the cystic $Pkd1^{V/V}$ mice regardless of the *Gpsm1* genotypes, but the BUN levels tended to be higher in the null *Gpsm1*-deficient $Pkd1^{V/V}$ mice. No difference was measured in the plasma (*D* and *E*) electrolytes, cyst fluid electrolytes (*F* and *G*), or the cyst fluid osmolality (*H*) between noncystic and cystic mice. All values are denoted as mean ± SEM. The numbers for each measurement are shown in the graph bars.

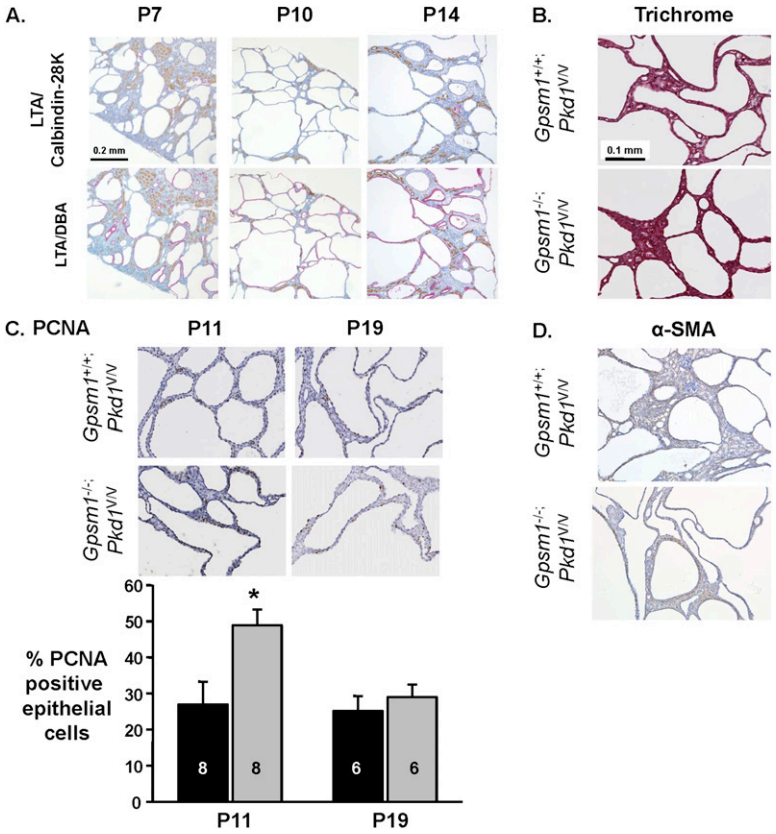

Fig. S3. Immunostaining of the *Pkd1*$^{V/V}$ kidney. (*A*) Kidneys were harvested from *Gpsm1*$^{+/+}$;*Pkd1*$^{V/V}$ mice at postnatal days 7 (P7), 10 (P10), and 14 (P14). Serial sections were made and stained with lectins specific for the proximal tubules (*Lotus tetragonobolus* agglutinin, brown), distal convoluted tubules (Calbindin-28K, red), and collecting duct epithelial cells (*Dolichos bifluorus* agglutinin, red). (*B*) Trichrome stain of kidney sections from *Gpsm1*$^{+/+}$;*Pkd1*$^{V/V}$ and *Gpsm1*$^{-/-}$;*Pkd1*$^{V/V}$ at postnatal days 11–12. (*C*) PCNA staining of kidney sections between *Gpsm1*$^{+/+}$;*Pkd1*$^{V/V}$ (black bars) and *Gpsm1*$^{-/-}$;*Pkd1*$^{V/V}$ (gray bars) at postnatal days 11–12 (P11) and 19 (P19). PCNA-positive cells were counted and calculated as a percentage of the total number of cystic epithelial cell nuclei (*Lower*). Although GPSM1 remains detectable at P19 in the *Gpsm1*$^{+/+}$;*Pkd1*$^{V/V}$ kidneys (Fig. S2*A*), the relative expression of GPSM1 at P19 compared with P11 is markedly lower. This may explain why the number of PCNA-positive cells is similar between the two groups at P19. The number of animals per group is shown in the graph bars. *$P < 0.05$: significant difference between the *Gpsm1*$^{+/+}$;*Pkd1*$^{V/V}$ and *Gpsm1*$^{-/-}$;*Pkd1*$^{V/V}$ mouse kidneys. (*D*) αSMA staining of *Gpsm1*$^{+/+}$;*Pkd1*$^{V/V}$ and *Gpsm1*$^{-/-}$;*Pkd1*$^{V/V}$ kidneys at P11. There were no observable differences in the red/blue staining pattern in *B* or in the amount of brown DAB staining in *D* for the αSMA between both mouse groups. No F4/80–positive cells, which are markers for macrophage infiltration, were detected in *Gpsm1*$^{+/+}$;*Pkd1*$^{V/V}$ and *Gpsm1*$^{-/-}$;*Pkd1*$^{V/V}$ kidneys (data not shown). (Scale bar: 0.2 mm in *A*; 0.1 mm in *B–D*.)

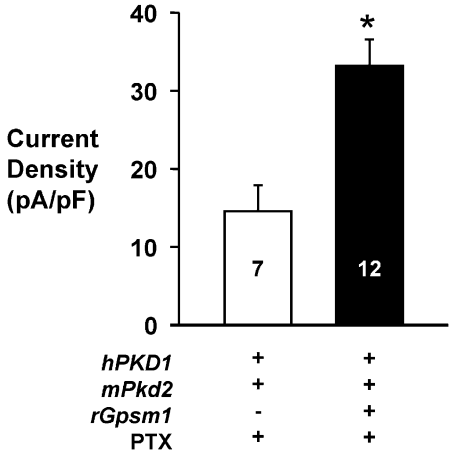

Fig. S4. Pertussis toxin does not block the GPSM1-mediated increase in PC1/PC2 current density. Summary graph of the La^{3+}-sensitive current density at –100 mV for voltage-clamped pertussis toxin (PTX)-treated CHO cells expressing *hPKD1* and *mPkd2* in the presence and absence of *rGpsm1*. In the presence of increased expression of GPSM1, Gαi subunits are scavenged and segregated from their Gβγ-binding partners. Subsequently, PTX is applied to the cells (200 ng/mL) for a period of 24 h before the measurement of the channel activity. Under these conditions, there is a significant increase ($P < 0.05$) in the channel density mediated by GPSM1 overexpression. Heterotrimeric G-protein cycling would still occur under PTX treatment, but would be independent of G-protein–coupled receptors activation. The high expression of GPSM1 would enable binding to the newly forming Gαi-GDP as it cycles from activation to inactivation and maintain the unbound pool of Gβγ dimers to promote increased channel activity. The number of observations in each group is shown in each bar. All values are denoted as mean ± SEM. *$P < 0.05$: significant difference between groups.